RESEARCH ARTICLE

Physiological and pathological high frequency oscillations in focal epilepsy

Jan Cimbalnik[1,2,a], Benjamin Brinkmann[1,3,a], Vaclav Kremen[1,3,4], Pavel Jurak[2,6], Brent Berry[1,7], Jamie Van Gompel[5], Matt Stead[1,3] & Greg Worrell[1,3]

[1]Mayo Systems Electrophysiology Laboratory, Department of Neurology, Mayo Clinic, 200 First St SW, Rochester, Minnesota 55905
[2]International Clinical Research Center, St. Anne's University Hospital, Brno, Czech Republic
[3]Department of Physiology and Biomedical Engineering, Mayo Clinic, 200 First St SW, Rochester, Minnesota 55905
[4]Czech Institute of Informatics, Robotics, and Cybernetics, Czech Technical University in Prague, Prague, Czech Republic
[5]Department of Neurosurgery, Mayo Clinic, 200 First St SW, Rochester, Minnesota 55905
[6]Institute of Scientific Instruments, The Czech Academy of Sciences, Brno, Czech Republic
[7]Department of Neurology, University of Minnesota, Minneapolis, Minnesota 55455

Correspondence

Greg Worrell, Department of Neurology, Mayo Clinic, 200 First St SW, Rochester MN, 55905. Tel/Fax: +1 507 538 9140; E-mail: worrell.gregory@mayo.edu

[a]Cofirst authors for this study

Abstract

Objective: This study investigates high-frequency oscillations (HFOs; 65–600 Hz) as a biomarker of epileptogenic brain and explores three barriers to their clinical translation: (1) Distinguishing pathological HFOs (pathHFO) from physiological HFOs (physHFO). (2) Classifying tissue under individual electrodes as epileptogenic (3) Reproducing results across laboratories. **Methods**: We recorded HFOs using intracranial EEG (iEEG) in 90 patients with focal epilepsy and 11 patients without epilepsy. In nine patients with epilepsy putative physHFOs were induced by cognitive or motor tasks. HFOs were identified using validated detectors. A support vector machine (SVM) using HFO features was developed to classify tissue under individual electrodes as normal or epileptogenic. **Results**: There was significant overlap in the amplitude, frequency, and duration distributions for spontaneous physHFO, task induced physHFO, and pathHFO, but the amplitudes of the pathHFO were higher ($P < 0.0001$). High gamma pathHFO had the strongest association with seizure onset zone (SOZ), and were elevated on SOZ electrodes in 70% of epilepsy patients ($P < 0.0001$). Failure to resect tissue generating high gamma pathHFO was associated with poor outcomes ($P < 0.0001$). A SVM classified individual electrodes as epileptogenic with 63.9% sensitivity and 73.7% specificity using SOZ as the target. **Interpretation**: A broader range of interictal pathHFO (65–600 Hz) than previously recognized are biomarkers of epileptogenic brain, and are associated with SOZ and surgical outcome. Classification of HFOs into physiological or pathological remains challenging. Classification of tissue under individual electrodes was demonstrated to be feasible. The open source data and algorithms provide a resource for future studies.

Introduction

Epilepsy surgery provides the best chance for seizure freedom for patients with drug resistant focal epilepsy,[1] but requires accurate localization and resection of the pathological tissue generating seizures at time of monitoring and in the future. Despite recording seizures with intracranial EEG (iEEG) to localize the seizure onset zone (SOZ), epilepsy surgery is often unsuccessful[1,2] and outcomes are difficult to predict.[3] On average, when considering temporal and extratemporal lobe epilepsy, approximately 50% of patients have recurrence of seizures after surgery.[1] Patients with normal MRI[1,4,5] are particularly challenging.

The effort to improve epilepsy surgery outcomes has led to intense interest in epileptogenic brain biomarkers that could identify tissue capable of generating seizures currently or in the future.[6] Many groups hypothesize that

interictal high frequency oscillations (HFO) in the local field potential are biomarkers of the pathological tissue responsible for seizure generation and at risk of epileptogenesis, and could be used to guide tissue resection and improve epilepsy surgery outcomes.[6–11] Interictal high-gamma (>65–100 Hz), ripple (>100–250 Hz) and fast ripple (>250–600 Hz) HFOs have each been implicated in seizure generation in humans.[8,10,12] Higher HFOs rates are reported in the SOZ,[13–21] and are correlated with disease severity.[22] Resection of tissue under electrodes with high HFO rates has been reported to correlate with seizure-free outcome.[19,23] High frequency oscillations (HFOs: 65–600 Hz), however, are also associated with normal brain physiology (see review[24]) and how to distinguish between pathological and physiological HFOs has remained unclear.[7]

Although HFOs are a promising electrophysiological biomarker of epileptogenic tissue, significant barriers to clinical translation remain: (1) HFOs are also associated with normal physiological function,[24–26] and it is currently unclear how to distinguish physiological HFOs (physHFO) from pathological HFOs (pathHFO).[7,27–29] (2) Epilepsy surgery requires classification of tissue under individual electrodes as pathological or normal. To date, the majority of investigations have simply shown that HFO rates are increased on average, when summed across all SOZ compared to non-SOZ electrodes (e.g. reviewed in[30]). (3) Reproducibility of published results has not been possible, as prior studies have relied on expert visual review or proprietary detectors, without making the data or computer code available to other investigators. (4) Lastly, previous studies investigating the association of pathHFO and epileptic brain have most often analyzed variably selected, short (<10 min) datasets, from relatively small numbers of patients, (e.g. $N = 9$,[13] $N = 19$,[14] $N = 6$,[16] $N = 7$,[17] $N = 10$,[18] $N = 9$,[31] $N = 20$,[19] $N = 30$,[32] $N = 35$,[27] $N = 54$[11]).

In this paper, we investigate HFOs as electrophysiological biomarkers for mapping epileptogenic brain, and address the technology gaps impeding clinical translation. The code and data are freely available so all reported results can be readily reproduced (http//:msel.mayo.edu).

Methods

Patients

112 consecutive patients were admitted to Mayo Clinic for prolonged iEEG monitoring as part of their evaluation for drug resistant focal epilepsy ($n = 100$) or facial pain ($n = 12$). Each patient consented to this Mayo Institutional Review Board approved study investigating wide bandwidth electrophysiology. The epilepsy patients were being evaluated for resective epilepsy surgery and the facial pain patients were implanted with intracranial electrodes for a trial of therapeutic motor cortex electrical stimulation.[33] The duration of clinical monitoring, and the location and number of implanted electrodes were determined solely by clinical considerations. Patient characteristics are summarized in Table 1.

Electrode implantation and localization

Implantation of depth and subdural electrodes was performed using methods described previously.[17,31] The depth electrodes (AD-Tech Medical Instrument Corp., Racine, WI or PMT, Chahassen, MN) are 4 or 8 Platinum/Iridium contacts (2.3 mm long, 1 mm diameter, and spaced 5 or 10 mm center-to-center). Subdural grids and strips are composed of 4.0 mm diameter Platinum/Iridium discs (2.3 mm exposed) with 10 mm center-to-center distance. Preimplantation MRI scan were fused with postimplantation high-resolution CT scans to localize electrodes using the Analyze (Biomedical Imaging Resource, Mayo Foundation, Rochester, MN) and Freesurfer.[26,34]

Intracranial EEG recording

The iEEG was recorded from depth and subdural electrodes using an inverted four contact strip placed in the epidural space for reference and ground. Clinical iEEG data were acquired at 500 Hz with a hardware filter 0.01–100 Hz (Natus Medical Incorporated Excel-Tech Ltd. (XLTEK) Oakville, Ontario, Canada). In parallel with the clinical data acquisition, research data were acquired using a splitter cable to couple to a Neuralynx system (Neuralynx Inc., Bozeman MT), and data sampled at 32 kHz with hardware filter bandwidth of DC – 9 kHz.[35] The research data were subsequently filtered by an antialiasing filter (Bartlett-Hanning window, 1 kHz) and down sampled to 5 kHz for further analysis. Visual review of individual channels was performed and channels with excess line noise (60 Hz), other artifacts, or containing no visible EEG signal were discarded prior to analysis. All clinical decisions were made based on review of the clinical XLTEK data.

Cognitive and Motor task induced physiological high frequency oscillations

Visual memory[26,36] and sensorimotor[28,37] laptop computer tasks were used to activate different brain regions involved in motor & memory function in 9 of the 100 epileptic patients as part of a protocol used for brain research (Fig. 1). Sensory-Motor task (4 patients): Patients used a keypad to log finger movements in response to visual

Table 1. Summary of patient characteristics.

Patients N = 102	Implanted contacts N = 13234	MRI	Surgical resection outcome	Pathology N
Epilepsy patients N = 90	# Electrodes = 6618 # Subdural = 5692 # Depth = 924	Abnormal: 58 Normal: 32	Total # 50 Engel 1: 31 Engel 2–5: 19	Gliosis = 51 MTS = 3 Inflammation = 17 Dysplasia = 10 Tumor = 1 Neuronal loss = 5 Encephalomalacia = 4
Temporal neocortex SOZ N = 30	# Electrodes = 1851 # Subdural = 1500 # Depth = 351	Abnormal: 21 Normal: 9	Engel 1: 7 Engel 2–5: 10	Gliosis = 19 MTS = 2 Inflammation = 6 Tumor = 1 Neuronal loss = 4
Temporal mesial SOZ N = 17	# Electrodes = 836 # Subdural = 471 # Depth = 365	Abnormal: 12 Normal: 5	Engel 1: 7 Engel 2–5: 1	Gliosis = 9 MTS= 1 Encephalomalcia = 1 Inflammation = 3 Dysplasia = 2
Frontal lobe SOZ N = 20	# Electrodes = 1803 # Subdural = 1761 # Depth = 42	Abnormal: 12 Normal: 8	Engel 1: 12 Engel 2–5: 5	Gliosis = 9 Encephalomalcia = 2 Fibrosis = 2 Inflammation = 3 Dysplasia = 7
Parietal lobe SOZ N = 4	# Electrodes = 270 # Subdural = 262 # Depth = 8	Abnormal: 3 Normal: 1	Engel 1: 0 Engel 2–5: 0	Gliosis = 2
Occipital lobe SOZ N = 1	# Electrodes = 116 # Subdural = 116 # Depth = 0	Abnormal: 0 Normal: 1	Engel 1: 0| Engel 2–5: 0	NA
Multifocal SOZ N = 18	# Electrodes = 1740 # Subdural = 1582 # Depth = 158	Abnormal: 10 Normal: 8	Engel 1: 5 Engel 2–5: 3	Gliosis = 12 Encephalomalcia = 1 Inflammation = 5 Dysplasia = 1 Neuronal loss = 1
Control patients Motor/sensory cortex N = 12	# Electrodes = 220 # Subdural = 92 # Depth = 128	Abnormal: 0 Normal: 12	NA	NA

Summary table with a summary of implantation sites, number of implanted contacts, surgical outcomes, and pathologies.

presentation of a finger name ("thumb", "index", etc.) or picture designating the finger to move on the keypad.[37] Visual Memory Tasks (5 patients): Patients were presented images from the International Affective Picture Set,[38] a collection of emotionally-laden images for memory processing (encoding, consolidation, & retrieval) as described previously.[26] The iEEG was recorded continuously and the timing of presentation and patient responses was relayed to the Neuralynx acquisition system by TTL pulse from the laptop computer and thus synchronized with iEEG recording. The data used for physHFO analysis were taken from non-SOZ areas and the channels visually checked for interictal epileptiform spikes (IES), electrographic seizures, and focal slowing, and if present the channels were excluded (N = 145) from further analysis.

Seizure onset zones

Clinical reports were used for SOZ localization. All clinically identified seizures were electronically imported as annotations into a custom viewer. In addition, a high sensitivity semiautomated seizure detection algorithm using signal line-length (LL) was run on all iEEG data and anomalous events identified.[39] Putative seizure detections and clinical annotations were visually reviewed (GW), and confirmed as clinical or subclinical electrographic seizures.
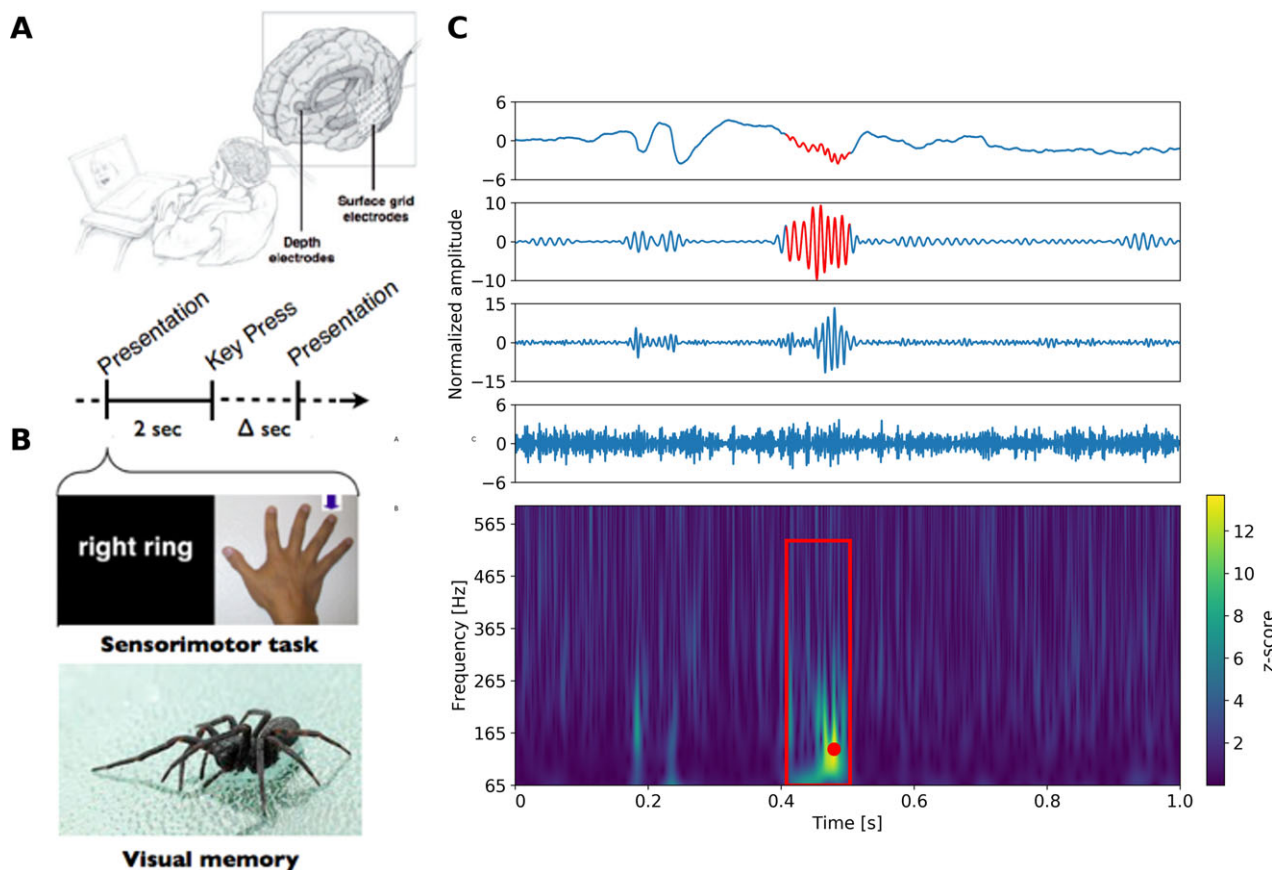
Figure 1. Task induced physiological high frequency oscillations (physHFO). (A) Schematic of patient performing laptop cognitive and motor tasks to induce physHFO associated with a physiological process. (B) Laptop computer presents finger name or picture of finger to move (right ring finger). The subject then toggles a keypad with the appropriate finger. Similarly, in the visual memory task the images are presented on a laptop for encoding and subsequent recall. Images are shuffled and mixed with foils during the recall task. (C) (*Top*) The upper panels show normalized raw data and band filtered data recorded (raw signal, high-gamma band, ripple band, fast ripple band – top to bottom). Red segment identifies automated HFO detection. (*Bottom*) Power spectrogram with Hilbert transform of 1 Hz filtered bands and z-scored signal. Significant HFO power increases (z-score >3.0) longer than three oscillations at frequency corresponding to the point with highest z-score shown as the red dot in the spectrogram. Red box identifies the bounding box of an automated HFO detection representing its spectral and temporal onsets and offsets.

The seizure onset time and electrodes involved at onset were determined by reviewing from a time of clear electrographic seizure activity backwards in time to the first visible change in the iEEG. Seizure onset channels and channels involved within 2.5 sec from seizure onset were marked as SOZ. In case of multiple SOZs the seizure onset channels from all seizures were labeled as SOZ and treated equally.

Irritative zones determination

Interictal epileptiform spikes (IES) were labeled using a previously validated automated detection algorithm.[40] Visual review of IES detections was used for validation. Channels with IES activity were annotated as Irritative zones (IZ). The detection algorithm evaluated each channel independently for IES, and no distinction was made between the spike maximum and spreading spikes.

HFO data analysis

Custom C and MATLAB (Mathworks, Natick, MA) program were used for data analysis.

Statistical software

All statistical tests were computed and visualized using Python libraries SciPy, Matplotlib.

Detection of task evoked physHFO (Fig. 1)

Significant HFO power increases were detected trial-by-trial using a previously published method[41] based on the

Hilbert transform applied across independently filtered bands. First, the trial data segment was band-pass filtered (Butterworth filter 5 taps with 1 Hz bands from 65 to 600 Hz, bands were then independently normalized by z-score transformation and plotted together on a time-frequency spectrogram.[26,28,36,41] Putative physHFO were identified as joined areas across all frequency bands with a z-score >3 on the spectrogram that were longer than three oscillations at the peak frequency which was identified as the point of the highest z-score within the joined area (Fig. 1C).[26] The bounding box of the area was used to determine physHFO onset and offset (Fig. 1C).

Detection of pathHFO (Fig. 2)

Detection of pathHFO events was performed using a multiple feature cascade detector with parameters selected based on detection of visually verified pathHFO in a training dataset, and then used without human intervention for analysis.[42] The automated detector was run on 2 h data segments taken from the first night of patient's stay at ICU between 1 and 3 AM. The data were band-pass filtered (Butterworth filter: 5 taps with frequency bands: 65–100 Hz, 100–250 Hz, 250–600 Hz, and 65–600 Hz). The following operations were carried out for each band-pass filtered dataset. The data were segmented into 10 second analysis windows. The features used for the cascade detection of pathHFO were: (1) Line-length (LL) was used as the first part of the cascade with low threshold setting (LL > mean(LL)$_{10}$ + 1.5 SD) to achieve high sensitivity detection of putative HFOs.[17,43] In each 10 sec window LL was calculated over a sliding detection window with length set to five oscillations at the low cut-off frequency plus ¼ window overlap. (2) Since pathHFO are
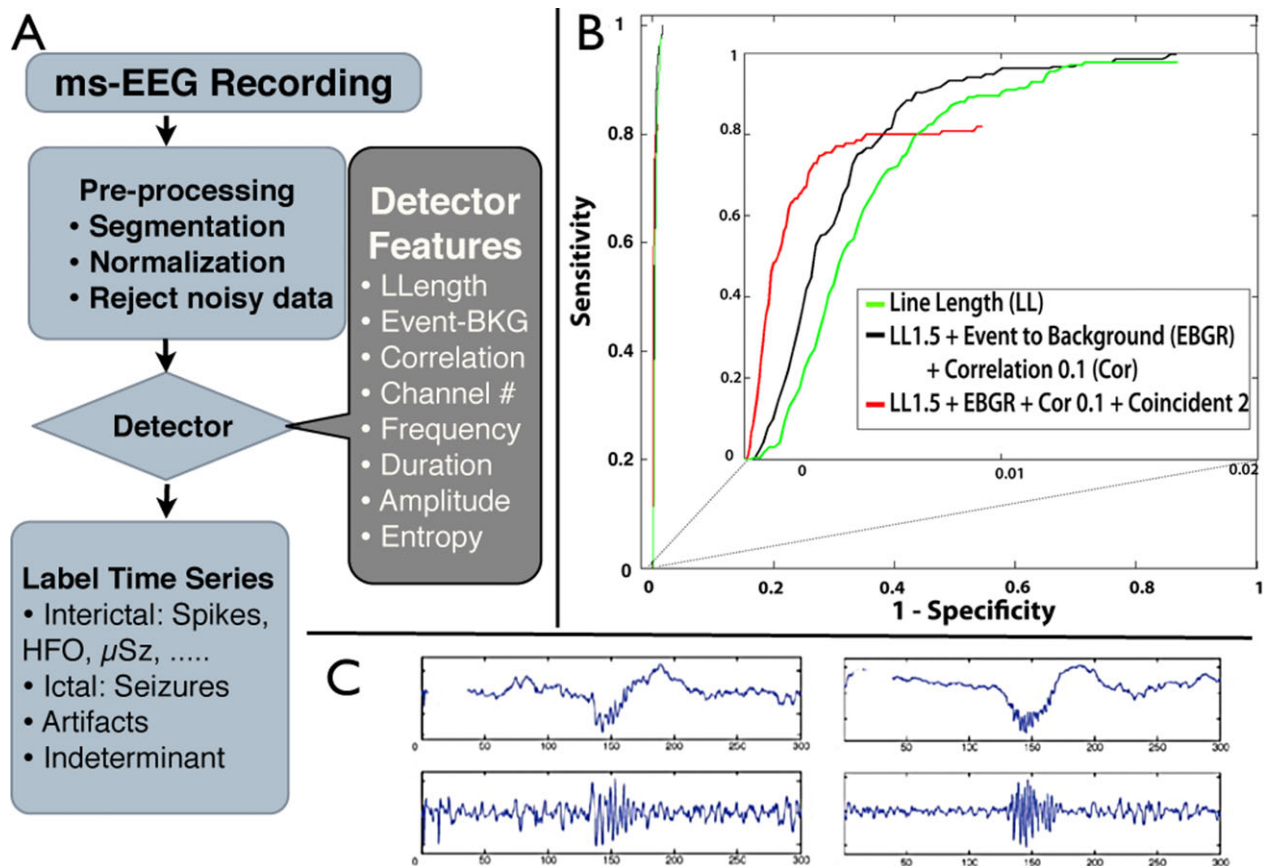

Figure 2. Automated cascade detector for pathological high frequency oscillations (pathHFO) (A) Schematic of multi-feature cascade pathHFO detector. Data are preprocessed (filtered, segmented, and demeaned). Artifact rejection removes data segments with high 60 Hz noise and anomalously high amplitudes. (B) Receiver-operator-curve (ROC) using "gold standard" pathHFO identified by expert visual review constructed by varying the threshold of event-to-background ratio. The ROC for multifeature cascade detector outperforms each single feature detector (inset shows ROC additional features improve performance). The performance of the pathHFO cascade detector shows improved sensitivity and specificity with each additional feature detector. (C) Exemplary pathHFO events. Raw data (top) & band passed filtered data (bottom).

focal events while artifacts often span many channels,[17,21,44] coincident events across >5 cm (5 macro contacts) with the same temporal onset time within 100 msec were discarded. (3) An event-to-background amplitude feature[45] was calculated as the ratio of average energy in the detected signal and the average energy of the surrounding 500 msec of data. (4) The maximum correlation of raw iEEG and band-pass filtered data was calculated for candidate events to exclude Gibbs filter artifact arising from sharp transient waveforms.[42,46]

Detector training

To optimize the parameters for pathHFO detection, the above features were calculated for "Gold standard" pathHFO events visually marked by expert reviewer in SOZ of patients with excellent postsurgical outcome (4 patients, 5 min segments, 21 channels, 7574 reviewed events). Receiver operating characteristic (ROC) curves were first calculated for each feature separately. The LL threshold was set to 1.5 standard deviations above the mean of the 10 sec analysis segment, which resulted in 99% sensitivity, but a high false positive rate which is acceptable for the initial cascade feature. Candidate events were excluded if the event to background ratio fell below 97% of cumulative distribution function (CDF) of candidate events. The correlation threshold was set to >0.1 for all but the Fast Ripple band (>250 Hz), in which the feature was omitted, as this value successfully eliminated events with high frequency power related to sharp transients without true oscillations.[42,46] Using the event-to-background feature as the threshold parameter, final ROCs were calculated for cascaded features (Fig. 2).

pathHFO detector validation

The detection process was validated on an independent data set (separate from the training data discussed above) of "gold standard" pathHFO detections using ROC and area under the ROC (AUC) (Fig. 2B). This held-out validation data set of expert reviewed pathHFO is comprised of 13,396 transient oscillations recorded from 22 electrodes in neocortex and medial temporal lobes from three subjects. To create the gold standard testing dataset visual review of raw and bandpass data was used to avoid inclusion of artifacts that show increases in high frequency power. Myogenic activity is well-known to interfere with the detection of HFO, and iEEG recordings are not immune to eye movement and muscle artifacts.[47] A 500 msec sliding window was used to score segments of signals. Any part of visually scored pathHFO present in the sliding window was considered to be a true positive while sliding windows without any HFO presence were

considered to be true negative. The performance of the pathHFO cascade detector in this validation dataset showed that each additional feature improved the detector's sensitivity and specificity (Fig. 2B).

Analysis of physHFO & pathHFO (Figs. 3 and 4)

The amplitude, frequency, and durations of physHFO and pathHFO detections were investigated in the broad band frequency range (65–600 Hz). Amplitude was calculated as mean amplitude of band pass filtered signal, duration as the difference between the onset and offset of the detection, and frequency determined based on the highest z-score value of the detection in spectrogram (Fig. 1). HFO event frequency, duration, and amplitude histograms are used to investigate evidence for characteristic oscillations and long-tail distributions. Task induced HFOs, HFOs spontaneously occurring in nonepilepsy patients and HFOs detected in SOZ of patients with excellent surgical outcome (Engel class I & ILAE 1) were compared with Wilcoxon rank sum test and Bonferroni correction was applied to address multiple comparisons. Detections exceeding the 99.9th percentile of the amplitude threshold were considered outliers and removed from analysis.

Analysis of pathHFO versus SOZ & non-SOZ (Fig. 5)

The pathHFO rates were obtained by counting detections in 10 min bins (pathHFO/10 min). The aggregate pathHFO rate in individual SOZ electrodes was compared with individual non-SOZ electrodes for all patients, including facial pain patients, using the Wilcoxon rank sum test and in individual epilepsy patients using a sign test for mean rate in SOZ electrodes and mean rate in non-SOZ electrodes. Statistically significant result was considered at the level of $\alpha = 0.95$. To investigate individual electrode classification as localized in the SOZ an ROC using SOZ contacts as true positives and non-SOZ contacts as true negatives was calculated by varying the pathHFO rate threshold. Since depth and subdural electrodes have different characteristics (impedance, shape, & target structure) statistical tests were also performed independently on neocortical & medial temporal contacts in a subanalysis.

Analysis of HFO rate and surgical outcome (Fig. 6)

Outcome of epilepsy surgery was evaluated using Engel outcome score and International League Against Epilepsy (ILAE) score. Only patients with more than 1 year after
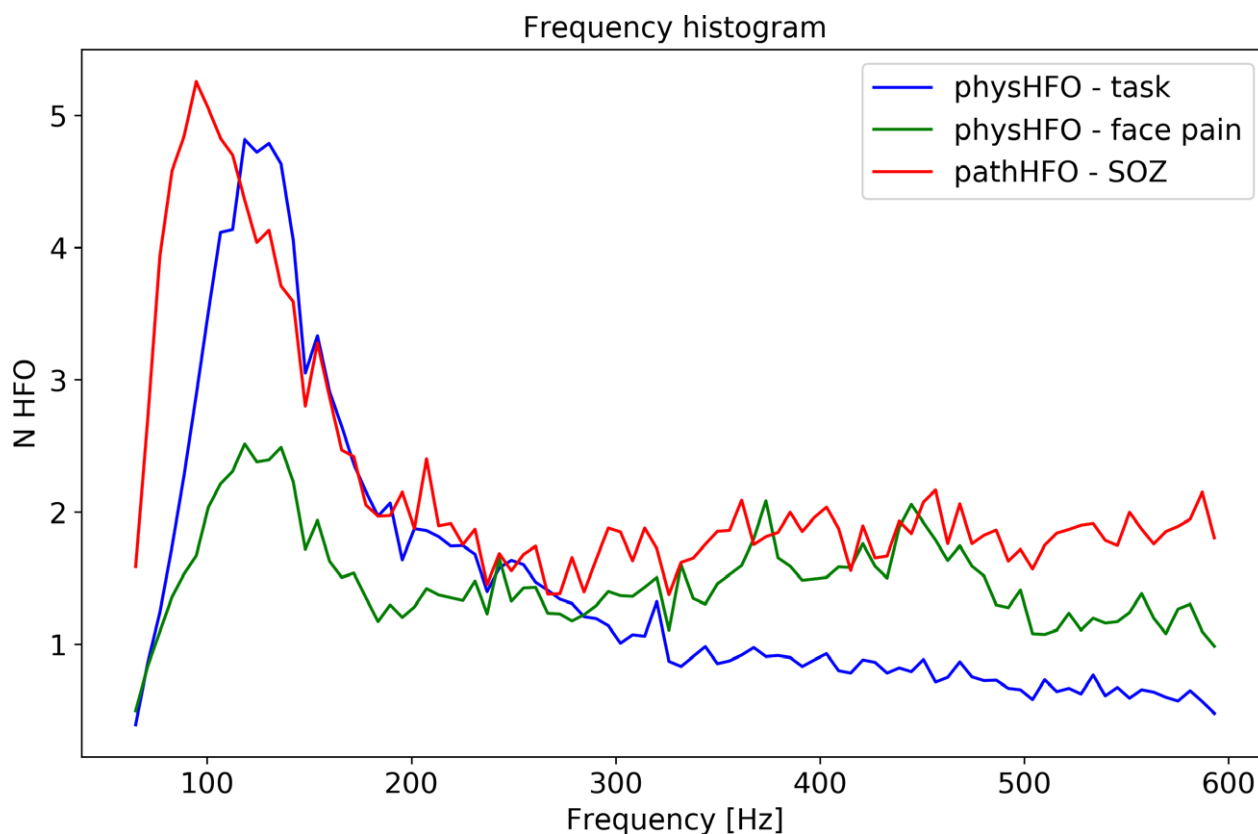
Figure 3. Distribution (histogram) of Physiological and Pathological High Frequency Oscillations (physHFO & pathHFO) Frequencies. The distribution of physHFO (blue = task induced outside seizure onset zone (nonSOZ), green = facial pain patients without history of seizures) and pathHFO (red = detected events inside the seizure onset zone (SOZ)) aggregated across patients with excellent outcome (ILAE = 1). The histograms of physHFO and pathHFO show distributions with a peak, characteristic or dominant oscillation frequency, in the high gamma to ripple frequency range.

the surgery were included and the most recent score was used in the analysis. Surgical records and postoperative MRI were used to determine whether the contacts were included in the resected tissue. The association of excellent outcomes with interictal pathHFO rates was investigated by comparing pathHFO (high gamma, ripple & fast ripple, wide bandwidth) rates in resected versus nonresected tissue.[19] Patients with excellent outcomes (Engel Class I & ILAE 1) were compared to patients with nonexcellent outcomes (Engel Class III & IV and ILAE 2–5) using the Wilcoxon rank sum test. Similarly to SOZ localization analysis, the statistical tests were carried out in neocortical & medial temporal contacts in subanalysis.

Support vector machine classifier (Fig. 7)

A support vector machine (SVM) classifier[48] (linear kernel) was used retrospectively to identify resected electrodes in 31 patients with excellent outcome (Engel Class I & ILAE 1) and resected tissue information available. The per-channel features included the pathHFO counts in

the high gamma, ripple, fast ripple, and broad (65–600 Hz) bands, pathHFO amplitude, over the 2-h data segments. In addition the contact type (depth vs. subdural grid/strip) was encoded and provided to the classifier. Features were normalized by converting to z-scores with mean and standard deviation (mean ± SD) computed within each patient's set of channels. The weight of nonresected electrodes (nonpathological data instances) and resected (pathological data instances) were adjusted inversely proportional to class frequencies in the input data for training. A leave-one-out cross validation was performed, testing performance on each patient in turns after training the SVM on the remaining patients. Mean sensitivity and specificity were calculated across the patient group, and the probability estimate that a channel data instance was assigned to the correct class was used to produce ROC curves. Mean ROC curve and its AUC were calculated on testing data. A Hanley-McNeil test[49] was used to compare classifier AUC to chance (AUC = 0.5). A similar procedure and feature set was used on a subgroup of 28 patients where MNI
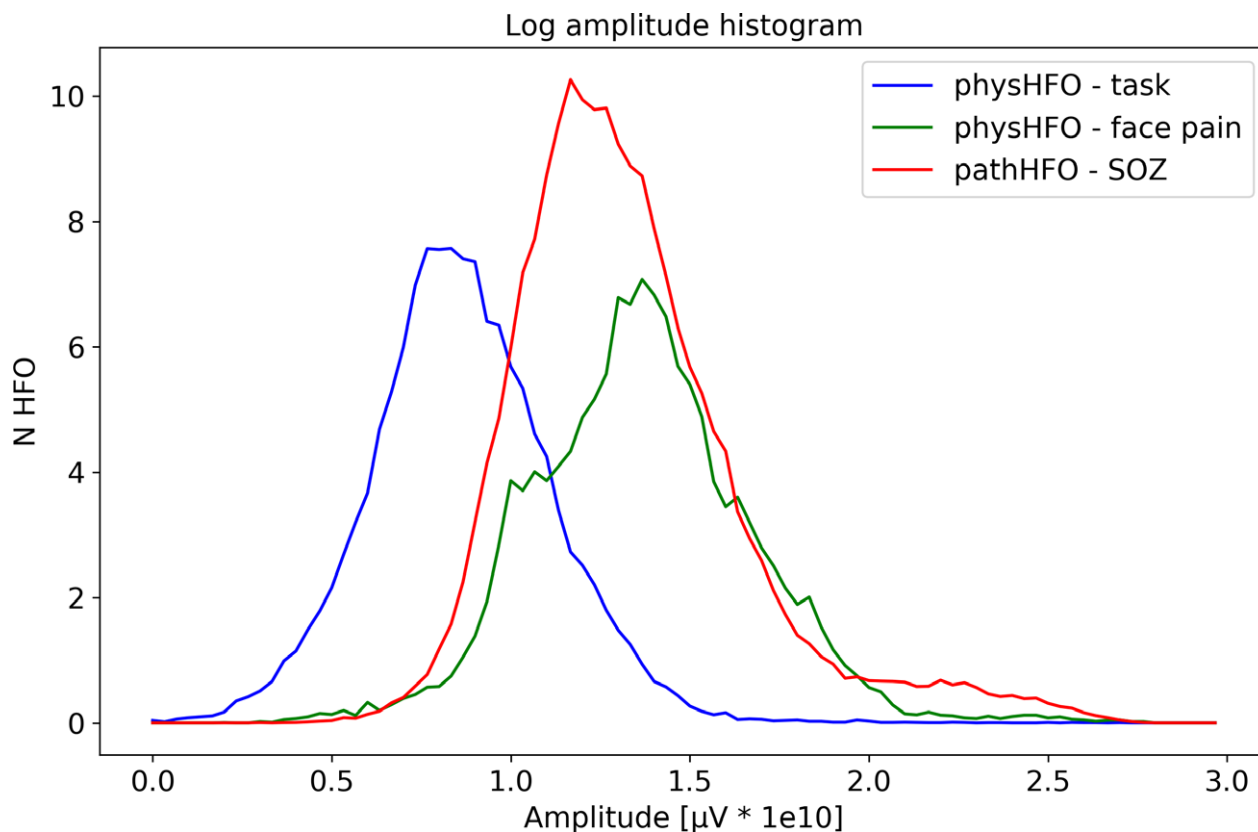
Log amplitude histogram

Figure 4. Distribution of Physiological and Pathological High Frequency Oscillations (physHFO & pathHFO) log amplitudes. The distribution of physHFO and pathHFO amplitudes overlap, but task induced physHFO (blue) are lower amplitude than seizure onset zone (SOZ) pathHFO ($P < 0.001$) and facial pain HFOs. Furthermore, the distribution of the pathHFO in SOZ has a long-tail distribution toward events at higher amplitude. The distribution of pathHFO events suggests pathHFO amplitude may be a useful feature for mapping SOZ and is incorporated in the support vector machine (SVM) model.

coordinates of electrode contacts were available and on a subgroup of 24 patients where a lesion in MRI image was identified and was used as a feature.

Results

Subjects and recordings

A total of 112 patients underwent wide bandwidth iEEG recordings. In 11 patients, the wide bandwidth research iEEG data quality was poor and these patients were excluded from further analysis. In the remaining 101 patients, 90 patients were undergoing iEEG for evaluation of drug resistant epilepsy and 11 patients were undergoing iEEG as part of a motor cortex stimulation protocol for drug resistant facial pain. The patient characteristics are listed in Table 1. Of the 101 patients analyzed, 34 patients were implanted with subdural electrodes only, 21 patients with depths electrodes only, and 46 patients implanted with a combination of subdural and depth electrodes. A total of 5582 subdural electrodes and 794

depth electrodes were analyzed. The mean length of the analyzed recordings was 7157.3 ± 312.8 sec. The mean number of contacts per patient was 64.7 ± 39.8.

Characteristics of physHFO & pathHFO (Figs. 3 and 4)

Physiological HFO were detected in the amygdala, hippocampus and neocortex, revealing discrete oscillations of characteristic frequency, duration latency, and spanning 65–600 Hz frequency band from nine epilepsy patients who underwent cognitive tasks[26,28,36] along with 11 patients with facial pain and no history of seizures. Feature histograms demonstrated long-tail distributions. The duration of physHFO, i.e. task induced HFOs and HFO in patients without history of seizures, was 0.022 ± 0.019 sec & 0.012 ± 0.012 sec ($P > 0.001$) respectively. The duration of HFO detected in SOZ of excellent outcome patients was 0.027 ± 0.023 sec and was statistically different from task induced HFO 0.023 ± 0.015 sec ($P < 0.001$) and HFO detected in facial
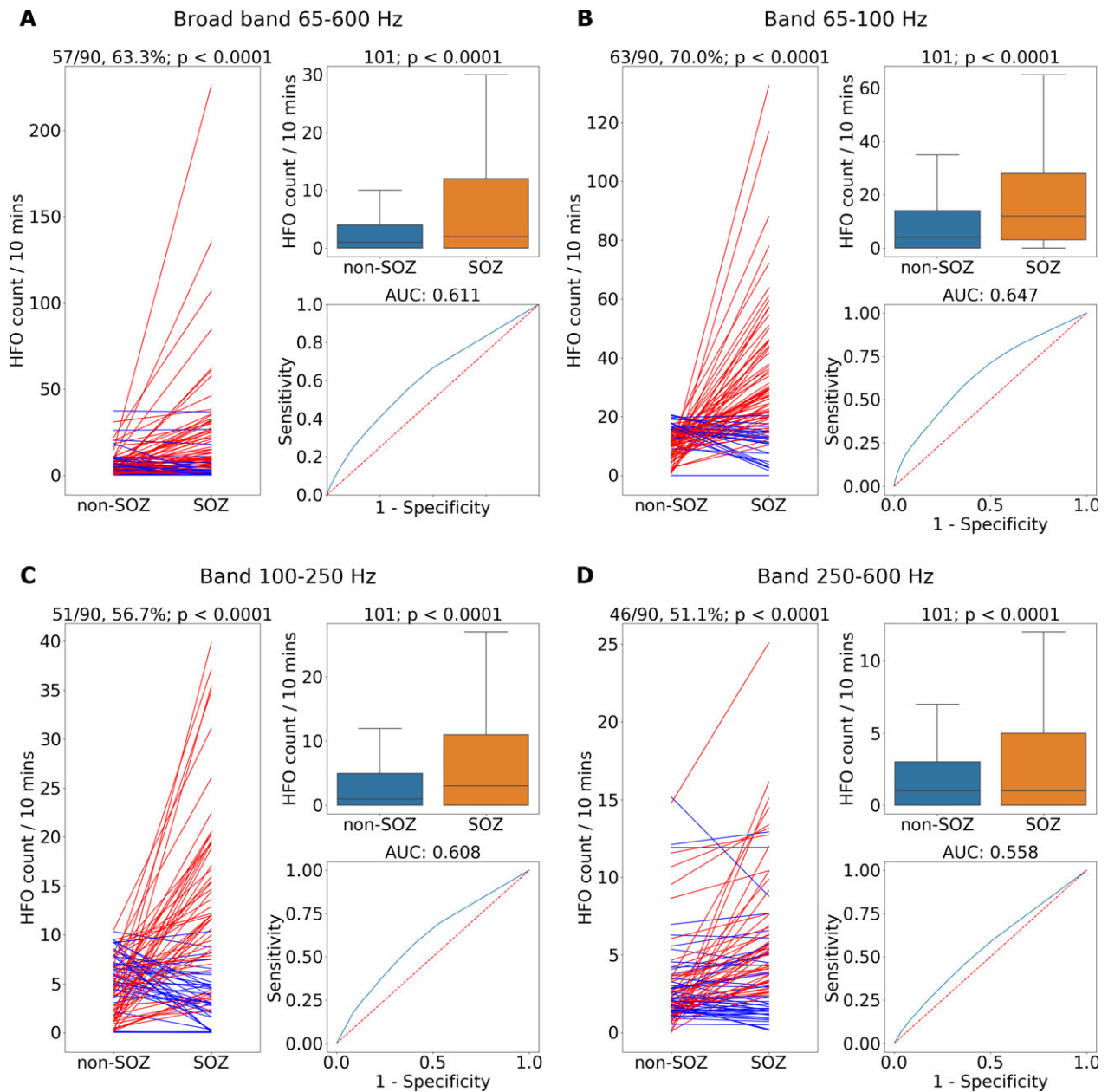
Figure 5. Pathological high frequency oscillations (pathHFO) are increased in seizure onset zone (SOZ). (A) Broad band pathHFO (65–600 Hz). (B) High gamma band pathHFO (65–100 Hz). (C) Ripple band pathHFO (>100–250 Hz). (D) Fast Ripple band pathHFO (>250–600 Hz). Left Panels (A–D): pathHFO rates (#counts/min-channel) are increased in SOZ versus non-SOZ for 63.3% (57/90, sign test $P < 0.0001$) of epilepsy patients for broad band, 70% (63/90, $P < 0.0001$) of epilepsy patients in high gamma, 56.7% (51/90, $P < 0.0001$) of epilepsy patients in Ripple, and 51.1% (46/90, $P < 0.0001$) of epilepsy patients in Fast ripple band. The lines represent mean HFO rate in non-SOZ and SOZ of individual patients where (red stands for $P < 0.05$, sign test). Upper Right Panels: pathHFO rates are increased in SOZ compared to non-SOZ ($P < 0.0001$) for all pathHFO bands when electrodes from all epilepsy and facial pain patients are aggregated ($N = 102$ patients, total electrodes = 6368, SOZ electrodes = 908, nonSOZ electrodes = 5460). Lower Right Panels: Receiver-operator-curve (ROC) and area-under-curve (AUC) for prospective individual SOZ versus non-SOZ electrode classification using the pathHFO band rates. The classification of individual electrodes as SOZ using pathHFO rates remains challenging, but most robust in the high gamma band. Note: the support vector machine (SVM) electrode classification using all four pathHFO bands combined with pathHFO amplitude yields a superior electrode classification to any of the individual pathHFO band results.
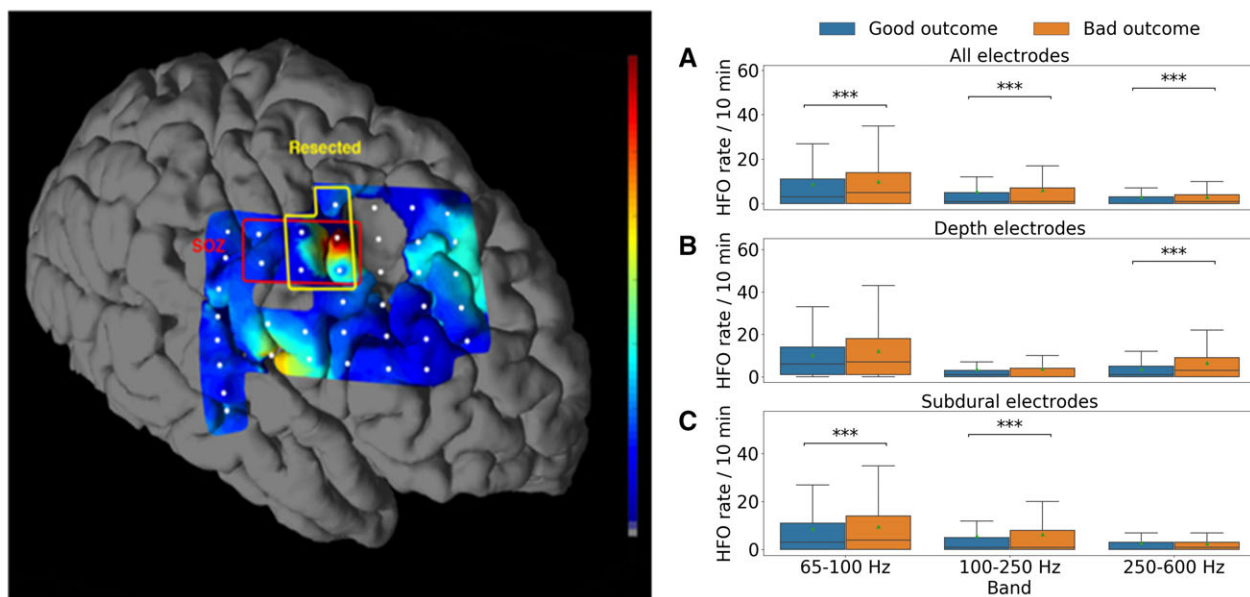
Figure 6. Unresected pathological high frequency oscillations (pathHFO) are associated with poor surgical outcome. Patients with unresected channels with increased pathHFO rates (#counts/min-channel) had unfavorable surgical outcomes. Left Panel: Representative patient. Coregistration of subdural electrodes onto pre-op MRI and postresection MRI. The SOZ and resected electrodes are identified. For visual display high gamma band pathHFO rate is interpolated between electrodes (normalized pseudo-color map). Right Panels: The aggregate rate of pathHFO from all unresected electrodes for all patients with excellent outcomes (Engel Class I) compared to patients with nonexcellent outcomes (Engel Class II & III & IV), $*P < 0.05$, $**P < 0.01$, $***P < 0.0001$. (A) High gamma, ripple, and fast ripple band pathHFO are associated with outcome ($P < 0.0001$). (B) Fast ripple band pathHFO are increased in unresected electrodes in mesial temporal structures ($P < 0.0001$). (C) High gamma and ripple band are increased in unresected subdural areas ($P < 0.0001$). The same analysis applied to interictal epileptiform spikes did not identify an association.

pain patients 0.018 ± 0.014 sec ($P < 0.001$) The amplitudes of task induced HFO, nonepileptic patient HFO and HFO detected in SOZ was 9.10 ± 9.01 & 31.94 ± 35.01 & 31.75 ± 46.29 μV ($P < 0.001$), respectively, where the histogram of pathHFO showed a distribution with long tail toward high amplitudes (Fig. 3). For all HFOs, physiological and pathological, there is a broad peak in the histogram in the high gamma frequency range. The largest peaks in the HFO frequency histograms were, pathHFO$_{peak}$ = 125.14 ± 34.51 Hz, task induced physHFO$_{peak}$ = 134.84 ± 30.94 Hz, and facial pain patient phyHFO$_{peak}$ = 133.60 ± 33.24. The distributions of the peaks were significantly different. Notably, the significance between task induced HFO and facial pain HFO was significant with very narrow margin ($P = 0.045$). There is, however, significant overlap of HFO distributions (Fig. 4) and long-tail distribution of events at higher frequency ranges.[28]

SOZ localization (Fig. 5)

Group analysis of pathHFO rate across the full data set (Fig. 5, $N = 102$ patients) revealed highly significant differences in SOZ and non-SOZ channels ($P < 0.0001$; Wilcoxon rank sum) in aggregate and in individual epilepsy

patients ($N = 90$, $P < 0.0001$, Sign test). The proportion of patients where the pathHFO rate in SOZ channels was significantly increased compared to non-SOZ channels was 63/90 for high-gamma, 51/90 for ripple, 46/90 for fast ripple, and 57/90 when considering broad band (all pathHFO) events (Wilcoxon rank sum for $P < 0.05$). ROC was calculated by varying the absolute HFO rate as a threshold which lead to AUC = 0.61. In the subgroup analysis of HFO rates in mesial temporal lobe epilepsy greater differences were observed between SOZ and non-SOZ electrode contact pathHFO rates ($P < 0.0001$; Wilcoxon rank sum) and in individual patients ($P < 0.0001$, 25/39, Sign test) compared to the subgroup of neocortical patients ($P < 0.0001$, 41/70, Sign test). Interestingly, gamma frequency pathHFO performed better for localizing SOZ than ripple pathHFO & fast ripple pathHFO and similar to previous studies, ripple pathHFO better localized the SOZ than fast ripple pathHFO.

HFO & surgery outcomes (Fig. 6)

In 61 of the 90 epilepsy patients conventional prolonged iEEG recordings (1–100 Hz) localized a surgically resectable focus that was used to guide surgical resection. Overall 61% (37/61) had excellent outcomes (Engel Class I &
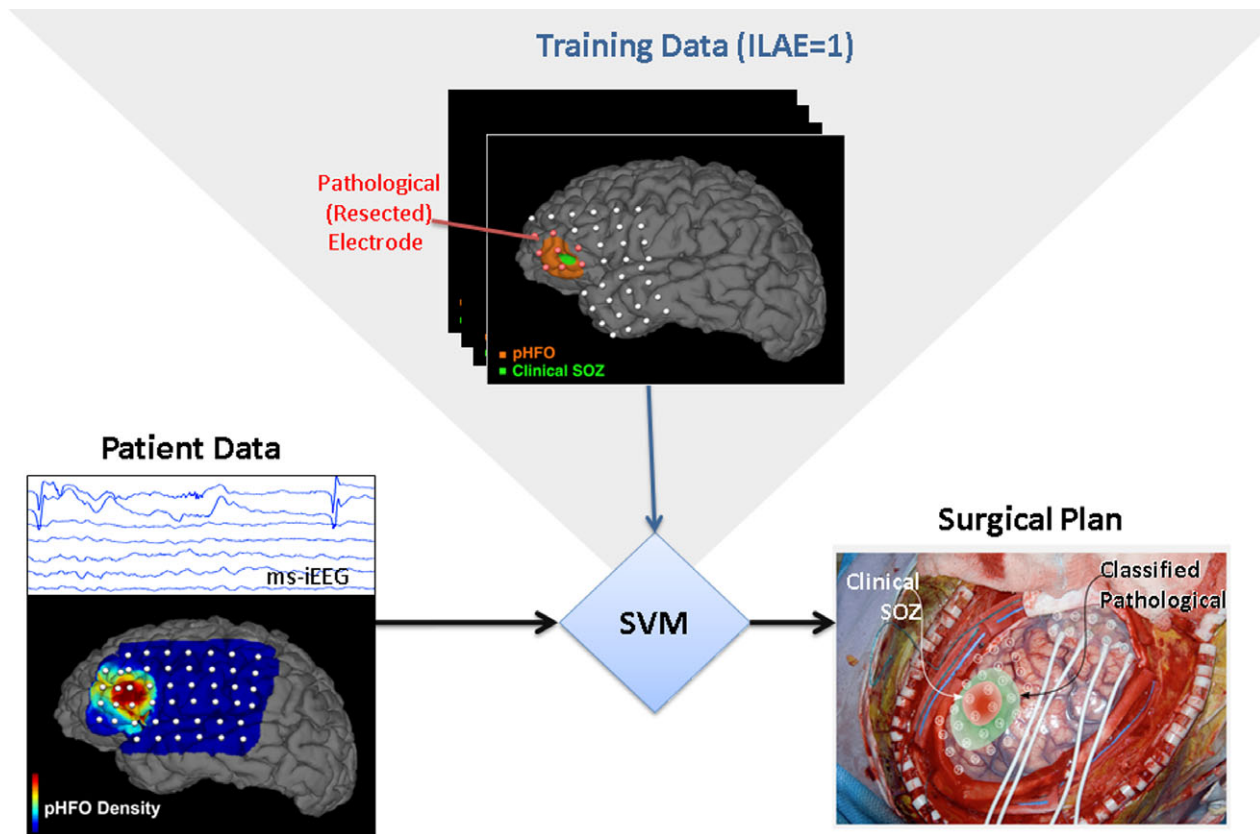
Figure 7. Support vector machine (SVM) classification of epileptogenic tissue. training data from 31 patients include multiple normalized pathHFO features for each electrode *(pathHFO rate, duration, amplitude)*. Here, SVM uses interictal iEEG data from excellent outcome patients (Engel I) for training. The SVM method uses the array of pathHFO features to train the classifier and then classifies each electrode as pathological (epileptogenic) or normal in an independent testing set ($N = 31$). In this example, the region of EZ determined by SVM extended beyond the SOZ determined iEEG recording of habitual seizures.

ILAE 1) at the last recorded follow-up. The aggregate rate of pathHFO from all unresected electrodes ($N = 4203$) showed significantly increased high gamma and ripple pathHFO ($P < 0.0001$) in patients with nonexcellent outcomes (Engel Class III & IV) compared to patients with excellent outcomes (Engel Class I). In the subanalysis of medial temporal contacts ($N = 407$) fast ripple pathHFO rates were significantly increased ($P < 0.0001$) whereas in the subanalysis of neocortical contacts ($N = 3796$) high gamma, ripple and fast ripple pathHFO rates ($P < 0.0001$) were significantly increased.

SVM classification of individual electrodes (Fig. 7)

Retrospective classification of channels using SVM resulted in a 0.685 AUC, 60.5% sensitivity and 66.7% specificity across the excellent outcome patient cohort ($N = 31$) and was significantly above chance ($P < 0.0001$). Addition of electrode MNI coordinates as a

feature in patients ($N = 28$) yielded an AUC of 0.721, with 63.7% sensitivity and 73.7% specificity. Further addition of an MRI-identifiable lesion to the feature set in a subset of patients ($N = 24$) with MRI lesions yielded AUC 0.728, 63.9% sensitivity and 73.7% specificity.

Discussion

A broader range of pathHFO (65–600 Hz) than previously recognized are shown to be biomarkers of epileptogenic brain, and associated with the SOZ and seizure free surgical outcomes when resected. This study used previously published and validated open-source detectors for mapping the rates of high-gamma, ripple, and fast ripple physHFO induced by tasks and spontaneous pathHFO in SOZ and non-SOZ tissue. The detectors were tuned to identify true oscillatory activity in iEEG and exclude high frequency components associated with sharp transients, i.e. "false HFOs" associated with Gibbs phenomena related to filtering sharp transients.[42,46]

The spectral and temporal characteristics of the pathHFO, spontaneous physHFO and task induced physHFO overlap, and they do not appear separable based on frequency or duration, but similar to previous pilot studies the pathHFO amplitudes are significantly higher compared to task induced physHFOs.[28] However, there is a notable long tail of pathHFOs in fast ripple range compared to physHFO, which suggests higher incidence of fast ripples in pathological tissue. In addition, the distribution of pathHFO amplitudes shows a long tail (Fig. 4) consistent with a gamma distribution with infrequent, high amplitude pathHFO events that are separable from physHFOs.[28]

In all analyzed frequency bands (high gamma, ripple, fast ripple, broad band) significantly higher pathHFO rates in aggregate across SOZ channels were confirmed, consistent with multiple previous studies (reviewed in[8–10]). The pathHFOs detected in low and high gamma band localized SOZ in a larger number of patients compared to ripple and fast ripple pathHFO. This could reflect higher specificity of ripples and fast ripples for highly localized seizure foci with higher rates occurring only in a subset of channels in the SOZ area.

Analysis of pathHFO rates in the unresected tissue in patients with excellent surgical outcome revealed a difference between neocortical and mesial temporal areas. In excellent outcome patients the resected tissue had higher pathHFO rates compared to tissue not resected. Conversely, for patients with poor post-resection seizure outcomes with a neocortical focus there were higher high-gamma and ripple rates in unresected areas than in resected areas. Fast ripples were significantly higher in unresected areas than in resected areas of mesial temporal brain structures in patients with poor post resection seizure outcomes. These results imply that the characteristics of pathHFOs might be different depending on the anatomical location of epileptogenic tissue, and warrants more investigation in the future.

Classification of tissue under individual electrodes as pathological is required for clinical translation and remains challenging using individual pathHFO rates and features. However, combining multiple pathHFO features (high-gamma, ripple, and fast ripple rates, HFO amplitude and electrode type) in an SVM classifier resulted in classification accuracy well above chance and shows promise for further development. Furthermore, introducing additional features acquired by imaging techniques (anatomical location and MRI-visible lesion) further improved classification performance (AUC = 0.72) providing evidence that integration of multiple diagnostic modalities into machine learning algorithms may ultimately prove clinically useful for localization of pathological brain.

Lastly, improvements in sensitivity and specificity for pathological tissue localization are still needed for clinical translation of pathHFO biomarkers for mapping epileptogenic tissue, but here the open source data, algorithms, and computer source code allows reproduction of all reported results and provides a resource for future studies.

The current study has a number of limitations, and in particular the use of SOZ or resected tissue in seizure free patients as the surrogate for pathological brain is problematic. Although this approach is common and the only viable approach currently, the substantial under-sampling of brain tissue by clinical iEEG recordings limits the definitive localization of the true onset of seizures compared to propagated seizure activity. In addition, the use of tissue resected in seizure free outcome patients as surrogate for pathological tissue is limited by the fact that successful epilepsy surgery is often associated with larger areas of resections and surgical margins, (e.g. the standard anterior temporal lobectomy amygdalohippocampectomy for temporal lobe) which almost certainly includes some nonpathological tissue not capable of independently generating seizures. The reproducibility of the results might be limited by different recording devices, electrodes, and clinical routines across laboratories.

Conclusion

There are physiologic HFOs (physHFOs) in all brain structures sampled and they occur within electrodes sampling both SOZ and non-SOZ. Similarly pathHFOs occur in both SOZ and non-SOZ and there is significant overlap in the spectral and temporal properties of physHFO and pathHFO. The distributions (histograms) of HFO amplitude, frequency, and duration for physHFO and pathHFO overlap significantly, suggesting that classification of HFO as physiological or pathological based on these features would be challenging. There is a trend toward pathHFO with significantly higher amplitudes, however, as evidenced by the long-tail of the pathHFO amplitude distribution. Nonetheless, pathHFOs rates identified using an unbiased, fully automated detector were demonstrated to be associated with the SOZ and seizure-free surgical outcomes. Thus, despite the fact that pathHFO and physHFO have similar characteristics there was a strong association of putative pathHFO with the SOZ and seizure free outcomes. Furthermore, by adding HFO amplitude and MRI features the classifier for identifying pathological brain tissue was improved. The findings here support the fact that HFO features, e.g. rate, amplitude, frequency, can be combined in a rigorous approach using a SVM classifier and achieve good performance. Classification of tissue under individual electrodes as pathological or normal based on HFO rates was relatively poor, but classification was

significantly improved by using multiple electrophysiological features extracted from automatically detected HFO events together with spatial information and MRI lesion information and shows potential for guiding epilepsy surgery. Lastly, based on these results improvements and further research on HFO characteristics with regard to anatomical location and well-designed prospective clinical trials are needed before widespread clinical translation of HFO biomarkers for mapping and resecting epileptogenic tissue is recommended. The open source data and source code provided allows replication of all results and provides a resource for future development and studies.

Acknowledgment

Author Contributions

B. Brinkmann, M. Stead, G. Worrell contributed to study concept and design. J. Cimbalnik, B. Brinkmann, J. Van Gompel, B. Berry, V. Kremen, P. Jurak contributed to data acquisition and analysis. J. Cimbalnik, B. Brinkmann, G. Worrell contributed to drafting the manuscript and figures.

Conflict of Interest

B. Brinkmann, G. Worrell, J. Van Gompel are recipients of grant funding from National Institute of Health (NIH R01-NS63039), during the conduct of the study.

G. Worrell, M. Stead, and J. Van Gompel own stock in Neuro One Inc.

B. Brinkmann, G. Worrell, J. Cimbalnik, B. Berry, V. Kremen are authors of a pending patent Seizure Onset Zone Localization With Bayesian Filtering And Subject Specific Feature Selection.

B. Brinkmann, G. Worrell are authors of a pending patent Multiscale Brain Electrode Devices And Methods For Using The Multiscale Brain Electrode.

V. Kremen is an author of a pending patent Platform for Automated Sleep Staging Using Intracranial Electrophysiology.

References

1. Téllez-Zenteno JF, Hernández Ronquillo L, Moien-Afshari F, Wiebe S. Surgical outcomes in lesional and non-lesional epilepsy: a systematic review and meta-analysis. Epilepsy Res 2010;89:310–318.

2. Najm I, Jehi L, Palmini A, et al. Temporal patterns and mechanisms of epilepsy surgery failure. Epilepsia 2013;54:772–782.

3. Jehi L, Yardi R, Chagin K, et al. Development and validation of nomograms to provide individualised predictions of seizure outcomes after epilepsy surgery: a retrospective analysis. Lancet Neurol. 2015;14:283–290.

4. Bell ML, Rao S, So EL, et al. Epilepsy surgery outcomes in temporal lobe epilepsy with a normal MRI. Epilepsia 2009;50:2053–2060.

5. Noe K, Sulc V, Wong-Kisiel L, et al. Long-term outcomes after nonlesional extratemporal lobe epilepsy surgery. JAMA Neurol. 2013;3:1–6.

6. Engel J. Biomarkers in epilepsy: introduction. Biomark Med. 2011;5:537–544.

7. Engel J, Bragin A, Staba R, Mody I. High-frequency oscillations: what is normal and what is not? Epilepsia 2009;50:598–604.

8. Worrell G, Gotman J. High-frequency oscillations and other electrophysiological biomarkers of epilepsy: clinical studies. Biomark Med. 2011;5:557–566.

9. Zijlmans M, Jiruska P, Zelmann R, et al. High-frequency oscillations as a new biomarker in epilepsy. Ann Neurol 2012;71:169–178.

10. Jacobs J, Staba R, Asano E, et al. High-frequency oscillations (HFOs) in clinical epilepsy. Prog Neurobiol 2012;98:302–315.

11. van't Klooster MA, vanKlink NE, Leijten FS, et al. Residual fast ripples in the intraoperative corticogram predict epilepsy surgery outcome. Neurology. 2015;85:120–128.

12. Staba RJ, Bragin A. High-frequency oscillations and other electrophysiological biomarkers of epilepsy: underlying mechanisms. Biomark Med. 2011;5:545–556.

13. Bragin A, Engel J Jr, Wilson CL, et al. High-frequency oscillations in human brain. Hippocampus. 1999;9:137–142.

14. Bragin A, Wilson CL, Staba RJ, et al. Interictal high-frequency oscillations (80-500 Hz) in the human epileptic brain: entorhinal cortex. Ann Neurol 2002;52:407–415.

15. Worrell GA, Parish L, Cranstoun SD, et al. High-frequency oscillations and seizure generation in neocortical epilepsy. Brain 2004;127(Pt 7):1496–1506.

16. Urrestarazu E, Jirsch JD, LeVan P, et al. High-frequency intracerebral EEG activity (100-500 Hz) following interictal spikes. Epilepsia 2006;47:1465–1476.

17. Worrell GA, Gardner AB, Stead SM, et al. High-frequency oscillations in human temporal lobe: simultaneous microwire and clinical macroelectrode recordings. Brain 2008;131(Pt 4):928–937.

18. Jacobs J, Levan P, Chander R, et al. Interictal high-frequency oscillations (80-500 Hz) are an indicator of seizure onset areas independent of spikes in the human epileptic brain. Epilepsia 2008;49:1893–1907.

19. Jacobs J, Zijlmans M, Zelmann R, et al. High-frequency electroencephalographic oscillations correlate with outcome of epilepsy surgery. Ann Neurol 2010;67:209–220.

20. Brázdil M, Halámek J, Jurák P, et al. Interictal high-frequency oscillations indicate seizure onset zone in patients with focal cortical dysplasia. Epilepsy Res 2010;90:28–32.

21. Crépon B, Navarro V, Hasboun D, et al. Mapping interictal oscillations greater than 200 Hz recorded with intracranial macroelectrodes in human epilepsy. Brain 2010;133(Pt 1):33–45.

22. Zijlmans M, Jacobs J, Zelmann R, et al. High frequency oscillations and seizure frequency in patients with focal epilepsy. Epilepsy Res 2009;85:287–292.

23. Wu JY, Sankar R, Lerner JT, et al. Removing interictal fast ripples on electrocorticography linked with seizure freedom in children. Neurology 2010;75:1686–1694.

24. Buzsáki G, Silva FLD. High frequency oscillations in the intact brain. Prog Neurobiol 2012;98:241–249.

25. Buzsaki G, Horvath Z, Urioste R, et al. High-frequency network oscillaiton in hippocampus. Science 1992;256:1025–1027.

26. Kucewicz MT, Cimbalnik J, Matsumoto JY, et al. High frequency oscillations are associated with cognitive processing in human recognition memory. Brain 2014;137 (Pt 8):2231–2244.

27. Wang S, Wang IZ, Bulacio JC, et al. Ripple classification helps to localize the seizure-onset zone in neocortical epilepsy. Epilepsia 2013;54:370–376.

28. Matsumoto A, Brinkmann BH, Stead SM, et al. Pathological and physiological high frequency oscillations in focal human epilepsy. J Neurophysiol 2013;110:1958–1964.

29. Alkawadri R, Gaspard N, Goncharova II, et al. The spatial and signal characteristics of physiologic high frequency oscillations. Epilepsia 2014;55:1986–1995.

30. Cimbalnik J, Kucewicz MT, Worrell G. Interictal high-frequency oscillations in focal human epilepsy. Curr Opin Neurol 2016;29:175–181.

31. Blanco JA, Stead M, Krieger A, et al. Data mining neocortical high-frequency oscillations in epilepsy and controls. Brain 2011;134(Pt 10):2948–2959.

32. Haegelen C, Perucca P, Châtillon C-E, et al. High-frequency oscillations, extent of surgical resection, and surgical outcome in drug-resistant focal epilepsy. Epilepsia 2013;54:848–857.

33. Lima MC, Fregni F. Motor cortex stimulation for chronic pain: systematic review and meta-analysis of the literature. Neurology 2008;70:2329–2337.

34. Fischl B. FreeSurfer. Neuroimage. 2012;62:774–781.

35. Brinkmann BH, Bower MR, Stengel KA, et al. Large-scale electrophysiology: acquisition, compression, encryption, and storage of big data. J Neurosci Methods 2009;180:185–192.

36. Matsumoto JY, Stead M, Kucewicz MT, et al. Network oscillations modulate interictal epileptiform spike rate during human memory. Brain 2013;136(Pt 8):2444–2456.

37. Whitmer D, Worrell G, Stead M, et al. Utility of independent component analysis for interpretation of intracranial EEG. Front Hum Neurosci. 2010;4:184.

38. Lang PJ, Bradley MM, Cuthbert BN. International affective picture system (IAPS): affective ratings of pictures and instruction manual. Technical Report A-8. 2008.

39. Gardner A, Krieger A, Vachtsevanos G, Litt B. One-class novelty detection for seizure analysis from intracranial EEG. Journal of Machine Learning Research. 2007;7:1025–1044.

40. Barkmeier DT, Shah AK, Flanagan D, et al. High inter-reviewer variability of spike detection on intracranial EEG addressed by an automated multi-channel algorithm. Clin Neurophysiol 2012;123:1088–1095.

41. Canolty RT, Edwards E, Dalal SS, et al. High gamma power is phase-locked to theta oscillations in human neocortex. Science 2006;313:1626–1628.

42. Worrell GA, Jerbi K, Kobayashi K, et al. Recording and analysis techniques for high-frequency oscillations. Prog Neurobiol 2012;98:265–278.

43. Gardner AB, Worrell GA, Marsh E, et al. Human and automated detection of high-frequency oscillations in clinical intracranial EEG recordings. Clin Neurophysiol 2007;118:1134–1143.

44. Bragin A, Mody I, Wilson CL, Engel J. Local generation of fast ripples in epileptic brain. J Neurosci 2002;22:2012–2021.

45. Blanco JA, Stead M, Krieger A, et al. Unsupervised classification of high-frequency oscillations in human neocortical epilepsy and control patients. J Neurophysiol 2010;104:2900–2912.

46. Bénar CG, Chauvière L, Bartolomei F, Wendling F. Pitfalls of high-pass filtering for detecting epileptic oscillations: a technical note on "false" ripples. Clin Neurophysiol 2010;121:301–310.

47. Kovach CK, Tsuchiya N, Kawasaki H, et al. Manifestation of ocular-muscle EMG contamination in human intracranial recordings. NeuroImage 2011;54:213–233.

48. Cherkassky V, Mulier FM. Learning from data: concepts, theory, and methods. Hoboken: John Wiley & Sons, 2007, 8.

49. Hanley JA, Mcneil BJ. The meaning and use of the area under a receiver operating characteristic (Roc) curve. Radiology 1982;143:29–36.

Supporting Information

Additional supporting information may be found online in the Supporting Information section at the end of the article

Figure S1. Correlation feature. Demonstration of correlation feature for reduction of false positive detection caused by Gibb's phenomenon. Top left: Simulated spike (orange) and surrounding signal (blue). Bottom left: Simulated HFO (orange) $f = 100$ Hz and surrounding signal (blue). Top right: Original spike (orange) and low-pass filtered (600 Hz cut-off) signal at the same position (blue). Bottom right: Original HFO (orange) and low-pass filtered (600 Hz cut-off) signal at the same position (blue). The corresponding correlation values are corr = 0.1 for spike and corr = 0.62 for HFO.

Figure S2. Unresected pathological high frequency oscillations (pathHFO) are associated with poor surgical outcome (1–1.5 year after resection). The aggregate rate of pathHFO from all unresected electrodes for all patients with excellent outcomes (Engel Class I) compared to patients with nonexcellent outcomes (Engel Class II & III & IV), *$P < 0.05$, **$P < 0.01$, ***$P < 0.0001$. The result corresponds to the result for all patients with the latest outcome after at least one year. Number of patients $N = 31$.

Table S1. Patient overview. Table with demographics and number of implanted electrodes and structures for individual patients. Highlighted patients were excluded from processing due to poor iEEG data quality.